Sticky-End Assembly of a Designed Peptide Fiber Provides Insight into Protein Fibrillogenesis†

Maya J. Pandya,‡ Gillian M. Spooner,‡,§ Margaret Sunde,‖ Julian R. Thorpe,‡ Alison Rodger,⊥ and Derek N. Woolfson*,‡

School of Biological Sciences, University of Sussex, Falmer, BN1 9QG, U.K., Department of Biochemistry, University of Cambridge, 80 Tennis Court Road, Old Addenbrookes Site, Cambridge, CB2 1GA, U.K., and Department of Chemistry, University of Warwick, Coventry, CV4 7AL, U.K.

Received February 2, 2000; Revised Manuscript Received May 8, 2000

ABSTRACT: Coiled-coil motifs provide simple systems for studying molecular self-assembly. We designed two 28-residue peptides to assemble into an extended coiled-coil fiber. Complementary interactions in the core and flanking ion-pairs were used to direct staggered heterodimers. These had "sticky-ends" to promote the formation of long fibers. For comparison, we also synthesized a permuted version of one peptide to associate with the other peptide and form canonical heterodimers with "blunt-ends" that could not associate longitudinally. The assembly of both pairs was monitored in solution using circular dichroism spectroscopy. In each case, mixing the peptides led to increased and concentration-dependent circular dichroism signals at 222 nm, consistent with the desired α-helical structures. For the designed fiber-producing peptide mixture, we also observed a linear dichroism effect during flow orientation, indicative of the presence of long fibrous structures. X-ray fiber diffraction of partially aligned samples gave patterns indicative of coiled-coil structure. Furthermore, we used electron microscopy to visualize fiber formation directly. Interestingly, the fibers observed were at least several hundred micrometers long and 20 times thicker than expected for the dimeric coiled-coil design. This additional thickness implied lateral association of the designed structures. We propose that complementary features present in repeating structures of the type we describe promote lateral assembly, and that a similar mechanism may underlie fibrillogenesis in certain natural systems.

The process of molecular self-assembly is central to all biological systems; it has implications for certain disease states (*1*) and applications in biotechnology (*2*) and nanotechnology (*3*). Arguably, the simplest and most ubiquitous self-assembling protein system is the α-helical coiled-coil (*4*). The basic sequence features that guide coiled-coil assembly are reasonably well understood (*5*, *6*). For instance, most coiled-coil sequences are dominated by a 7-residue repeat of hydrophobic (H)[1] and polar (P) residues, $(HPPHPPP)_n$, known as the heptad repeat. When configured into α-helices, these patterns give amphipathic structures, the hydrophobic faces of which direct oligomer assembly. The number of chains within a coiled-coil bundle—that is, its oligomer state—is determined predominantly by the nature of residues at "H", which form the core of the structure (*5*−*7*). In addition, residues that flank the core can have charged side chains that contribute to partner selection; that is, these residues help determine partners in hetero-oligomeric structures (*8*−*10*). Our understanding of these structures has come largely from small leucine zipper-like motifs, and this has led to successful peptide designs (*11*−*15*). Most natural coiled-coils, however, form extended structures hundreds or thousands of residues in length. Furthermore, many associate into high-order assemblies (*4*, *16*). Examples range from rope-like structures such as intermediate filaments (*16*, *17*) to relatively complicated organelles such as the spindle pole body (*18*).

Throughout biology there are many examples of complicated, high-order assemblies other than coiled-coils. Unlike natural coiled-coils, which to our knowledge are all in-register structures with flush or "blunt" ends, many of these structures assemble by staggering protein subunits. Examples include the packing of peptides in certain viral coats (*19*) and the assembly of G-actin into F-actin fibers (*20*). Similar examples also occur in the association and high-order assemblies of folded coiled-coil units: the end-to-end overlap within tropomyosin filaments (*21*) and the side-to-side aggregation of coiled-coils within myosin filaments (*22*). In addition, it is likely that the assembly of intermediate filaments initially involves staggering coiled-coil dimers to form tetramers (*17*).

† Supported by the Biotechnology and Biological Sciences Research Council of the U.K. and the Wellcome Trust. M.S. is a Royal Society University Research Fellow.

* Corresponding author. E-mail dek@biols.susx.ac.uk; Fax +44 (0)-1273 678433.

‡ University of Sussex.

§ Present address: The Haemophilia Centre, Coagulation Research Laboratory, St. Thomas' Hospital, Lambeth Palace Rd., London, SE1 7EH, U.K.

‖ University of Cambridge.

⊥ University of Warwick.

[1] Abbreviations: CD, circular dichroism; H, hydrophobic; LD, linear dichroism; P, polar; SAF-p, self-assembling fiber peptide; SEM, scanning electron microscopy; TEM, transmission electron microscopy.

10.1021/bi000246g CCC: $19.00
Published on Web 06/30/2000

Motivated by the staggering of subunits in natural structures, we designed two 28-residue peptides to form initially a staggered heterodimer that acts as a seed to promote the assembly of extended coiled-coil fibers. We used a combination of peptide synthesis, spectroscopy, and electron microscopy to test and demonstrate this design. The same principle of using complementary "sticky-ends" is well established in molecular biology for assembling DNA (*23*) and has been used to design intricate DNA crystals (*24*). However, we believe our application of sticky-end-directed molecular assembly for peptides is new. We do note that head-to-tail packing of helices has been observed in recently solved crystal structures for two designer peptides (*25, 26*), and that fibrous structures have been produced serendipitously from a peptide originally designed to form a four-helix bundle (*27*).

EXPERIMENTAL PROCEDURES

Peptide Synthesis. Peptides were synthesized on an Applied Biosystems 432A Peptide Synthesizer using solid-phase methods and Fmoc chemistry. Peptide samples were purified using reversed-phase high-performance liquid chromatography, and their identities were confirmed by MALDI-TOF mass spectrometry.

Computer Modeling. A model for the three-dimensional structure of the designed protein fiber was made from the minimized structure of a model coiled-coil 35-mer, $(LAALAAA)_5$, that was generated using the Crick equations (*28*). Copies of the 35-mer were superimposed with an overlap of one heptad repeat to extend the structural template, and the backbone was rejoined after removal of overlapping segments. Residues in the two-stranded template were replaced with the sequences of the SAF peptides, staggered relative to each other by two heptad repeats according to the alignment in Figure 1a. The structure was soaked in a 5 Å layer of water and energy-minimized until the average absolute derivative of coordinates with respect to energy fell below 0.01 kcal $Å^{-1}$. The structure was built and visualized using Insight II 97.0 (Molecular Simulations Inc.), and was energy-minimized using Discover 2.9.8 (Molecular Simulations Inc.) with the consistent valence force field.

Spectroscopy. Peptide samples were examined at 5 °C in 10 mM MOPS [3-(*N*-morpholino)propanesulfonic acid], pH 7. Sample concentrations were determined from their UV absorbance at 280 nm (SAF-p1) and 214 nm (SAF-p2). After baseline correction, ellipticities in millidegrees were converted to molar ellipticities (degrees centimeter squared per decimoles of residue) by normalizing for the concentration of peptide bonds. Data were recorded in a cell of 1 mm path length by integrating the signal for 5 s (and 1 s for the fresh 100 μM peptide mixture) every nanometer in the range 205−260 nm. CD measurements were made using a JASCO J-715 spectropolarimeter fitted with a Peltier temperature controller. LD data were recorded using a JASCO J-715 spectropolarimeter adapted for the purpose with samples housed in a couette flow cell (*29*) with a path length of 1 mm. Orientation of the fibers was achieved by shear flow, that is, viscous drag of the sample between a fixed outer cylinder and a rotating solid quartz inner cylinder. Spectra were measured by averaging the signal for 2 s every nanometer in the range 210−320 nm. After baseline correction, absorbance was converted to molar extinction coefficient (l mol·res^{-1} cm^{-1}) by normalizing for the concentration of peptide bonds. A linear correction for a sloping baseline was made to the data from the 100 μM SAF peptide mixture.

Sedimentation Equilibrium Ultracentrifugation. Sedimentation equilibrium experiments were conducted at 5 °C in a Beckman-Optima XL-I analytical ultracentrifuge using an An-60 Ti rotor. One hundred microliter samples of a 100 μM mixture of SAF-p2 and SAF-p3, which gave an initial A_{280} value of 0.14 in the 1.2 cm path length ultracentrifugation cell used, were buffered to pH 7 with 10 mM MOPS, 100 mM sodium chloride. Samples were equilibrated for about 48 h at speeds of 30 000 and 40 000 rpm, and sedimentation equilibrium curves were measured by the absorbance at 280 nm. Data were fitted simultaneously using routines in the Beckman-Optima XL-A/XL-I data analysis software (v4.0), which employs a nonlinear least-squares method of Johnson et al. (*30*). The density of the buffer at 5 °C was taken to be 1.004 mg/mL, and the averaged partial specific volume for the SAF peptides calculated on the basis of amino acid composition was 0.749.

X-ray Fiber Diffraction. Mixtures of SAF peptides at 500 μM in 10 mM MOPS, pH 7, were incubated on ice for at least 1 h, before centrifugation at 6500*g* for 5 min. Droplets of fiber-containing solutions, taken from the bottom of the centrifuged tubes, were suspended between the ends of two wax-filled capillaries and allowed to dry slowly overnight at 4 °C, yielding clumps of partially aligned fibers (*31*). X-ray fiber diffraction images were collected using a Rigaku CuKα rotating anode source (wavelength 1.5418 Å) and a R-AXIS IV detector. Samples were maintained at 5 °C during data collection with cool air from a cryostream (Oxford Cryosystems).

Electron Microscopy. For most TEM experiments, a drop of peptide solution was applied to a carbon-coated copper specimen grid (Agar Scientific Ltd., Stansted, U.K.), and dried with filter paper before negative staining with filtered (0.22 μm) 0.5% aqueous uranyl acetate and then dried at 5 °C. Peptide samples in filtered 10 mM MOPS, pH 7, were incubated on ice for 1 h beforehand. "Fresh" SAF peptide mixtures were prepared by mixing preincubated solutions of the individual peptides at 200 μM directly on the specimen grid, before drying and negative staining. Grids were examined in a Hitachi 7100 TEM at 100 kV, and digital images were acquired with a (800 × 1200 pixel) charge-coupled device camera (Digital Pixel Co. Ltd., Brighton, U.K.) and analyzed (Kinetic Imaging Ltd., Liverpool, U.K.). For SEM experiments, negatively stained specimen grids were sputter-coated with gold and examined in a Leo Stereoscan 420 SEM at 20 kV and with a probe current of 10 pA.

RESULTS

Peptide Design. With the goal of making elongated structures to improve our understanding of coiled-coils and to develop new designer structures, we designed two 28-residue synthetic peptides—dubbed Self-Assembling Fiber peptides, SAF-p1 and SAF-p2—to fold and form extended fibers when mixed (Figures 1 and 2). The building block of the design was a staggered heterodimer with overhanging ends. This contrasts with the natural and designer coiled-

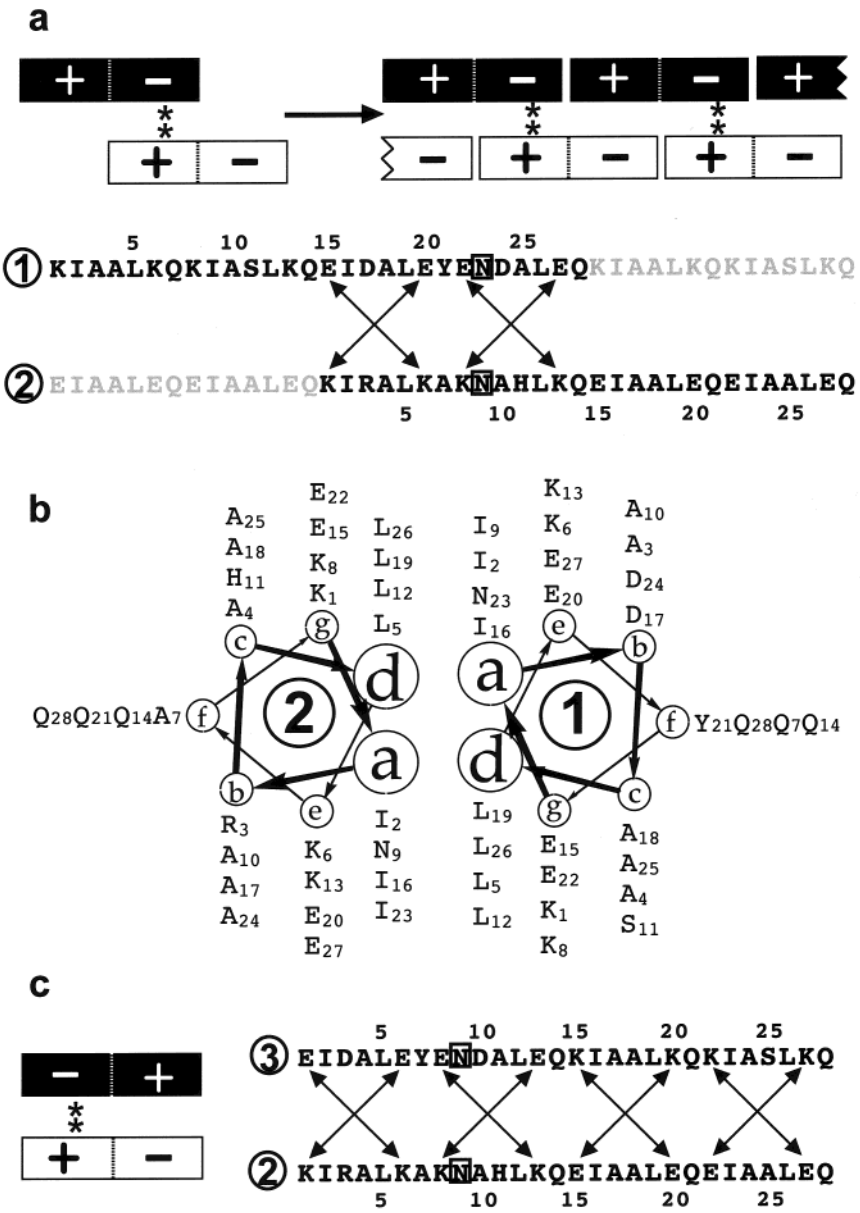

FIGURE 1: Design and sequences of the self-assembling fiber (SAF) peptides. (a) Concept for a sticky-end assembly process together with the designed amino acid sequences. Complementary charges in companion peptides direct the formation of staggered, parallel heterodimers; the resulting "sticky-ends" are also complementary and promote longitudinal association into extended fibers. Circled numbers represent the relevant peptide number, asterisks represent asparagine residues, and arrows represent complementary electrostatic interactions. (b) Helical-wheel representation summarizing the designed sequences in context. The view is from the N-terminus with heptad sites labeled *a*−*g* and is simplified by using 3.5 residues per helical turn. (c) Amino acid sequences designed to form blunt-ended heterodimers; sequence 3 is a permutation of sequence 1.

coils characterized to date, that have flush, or blunt, ends. Staggering was achieved by focusing on the buried, hydrophobic-core positions of the structure. Existing rules were incorporated at the dimer interface to direct formation of the desired parallel staggered dimer, and to guard against alternative oligomers and topologies (*5*, *6*, *32*). Complementary core interactions and flanking ion-pairs were incorporated into the overhangs to facilitate longitudinal association of the heterodimers (Figures 1 and 2).

Specifically, each peptide comprised canonical heptad repeats (***abcdefg***) with isoleucines at ***a*** and leucines at ***d*** to ensure coiled-coil dimers (*5*, *6*). Oppositely charged glutamate and lysine residues were incorporated at ***e*** and ***g*** (*33*) to favor the staggered dimer with sticky-ends. In addition, to cement the prescribed register further and to favor parallel structures, asparagine residues, which preferentially pair with each other at ***a*** sites in coiled-coil dimers (*6*, *12*, *32*, *34*), were included in different, complementary heptads of the two peptides (Figure 2a). A third peptide, SAF-p3, was designed as a circular permutation of SAF-p1 with residues 15−28 swapped for residues 1−14. This peptide should interact with SAF-p2 according to Figure 1c, resulting in heterodimers with blunt ends that cannot associate longitudinally. All three peptides were synthesized and studied using spectroscopic techniques and microscopy.

We refer to the combination of peptides SAF-p1 with SAF-p2 as the fiber-producing mixture, and the combination of peptides SAF-p2 with SAF-p3 as the blunt dimer-producing mixture.

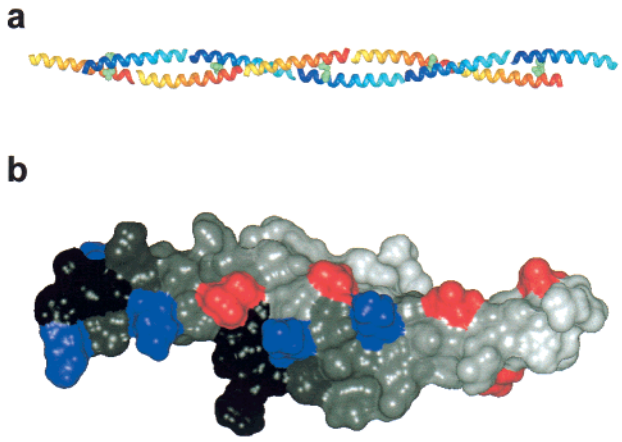

FIGURE 2: Computer modeling of the designed self-assembling fiber. (a) SAF-p1 (colored yellow-to-red from the N- to the C-terminus) and SAF-p2 (colored blue-to-cyan from the N- to the C-terminus) interact through core residues including asparagine pairs (colored green) to form the two strands of a staggered, parallel, coiled-coil fiber. (b) Negatively charged glutamate side chains (colored red) and positively charged lysine side chains (colored blue) form complementary charge interactions between SAF peptides. For clarity in this panel, both SAF peptides are shaded dark to light gray from their N-terminus to the C-terminus.

Circular Dichroism Spectroscopy. Consistent with our design, neither SAF-p1 nor SAF-p2 was highly structured in aqueous solution at pH 7 and 5 °C (Figure 3). However, when mixed in equal proportions, to give the fiber-producing mixture, the circular dichroism (CD) spectrum changed and, moreover, was markedly different from the theoretical spectrum generated by averaging the spectra for the isolated peptides. CD spectra for α-helical structures are characterized by intense minima at 208 and 222 nm. These features, particularly the signal at 222 nm, were pronounced in the spectra of the SAF mixtures, but were much less evident in the spectra of the individual peptides (Figure 3a,b). The shape and intensity of spectra from 100 μM fiber-producing mixtures (SAF-p1 and SAF-p2) also changed with time (Figure 3b). Spectra recorded immediately after mixing—dubbed "fresh" samples—displayed some α-helical structure. However, after incubating the mixture for 1 h at 5 °C—"maturation"—the signal at 222 nm doubled in intensity while the signal at 208 nm remained almost unaltered. This may appear inconsistent with α-helical proliferation. However, the red shifting and dampening of signal toward lower wavelengths in spectra that we observed is most probably due to light scattering and flattening distortions that are commonly seen in particulate systems (*35*). We note that similar effects have been observed during the self-assembly of RecA (*36*). In this case, the authors report an increase in turbidity of the RecA solution upon association. Indeed, in our case, the changes in the CD spectra for 100 μM fiber-producing mixtures were accompanied by slight clouding of the solution. Brief centrifugation of these mixtures after maturation established that the CD signal derived largely from the suspended material. In addition, and as expected for a multimerization event, we found that the magnitude of the mature CD signal depended on peptide concentration; a fiber-producing mixture with 100 μM of each peptide gave a much stronger signal than a 10 μM mixture (Figure 3a,b).

As a control, SAF-p3 (the permutation of SAF-p1) was designed to form a blunt-ended heterodimer with SAF-p1

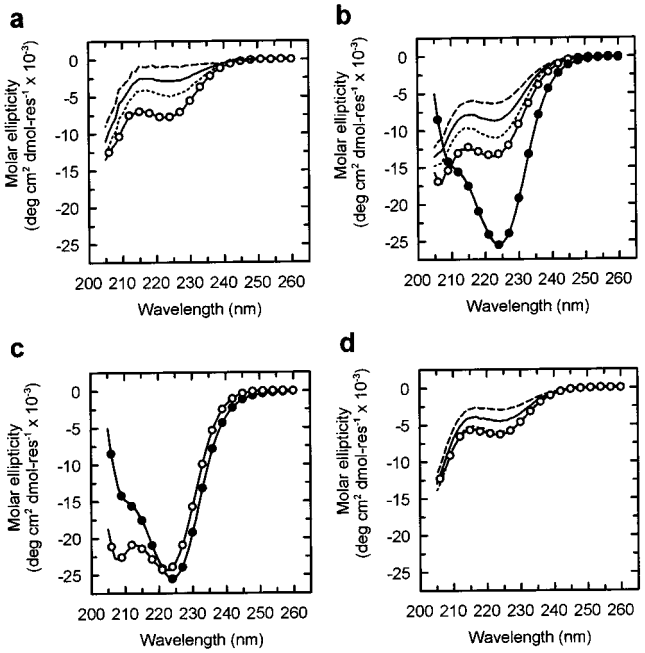

FIGURE 3: Spectroscopic evidence for the formation of high-order helical structures by the SAF peptides. (a) Circular dichroism (CD) spectra at 10 μM for SAF-p1 (— —), SAF-p2 (---), the average of these spectra (—), and the experimental SAF peptide mixture (○). (b) CD spectra for SAF-p1 and SAF-p2 at 100 μM. The key is the same as for part a, but with an additional spectrum (●) for the SAF peptide mixture after "maturation" for 1 h. (c) CD spectra of matured fiber-producing (SAF-p1 with SAF-p2) (●), and blunt-dimer producing (SAF-p2 with SAF-p3) (○) mixtures at 100 μM. (d) CD spectra for SAF-p1 and SAF-p2 at 100 μM in 0.5 M KF; the key is the same as for part a. For clarity, only a fraction of the experimental data points are highlighted by the symbols (●) and (○).

that should not assemble further into fibers. 100 μM mixtures of SAF-p2 and SAF-p3 were analyzed by sedimentation equilibrium in the analytical ultracentrifuge. The resulting data were best fitted assuming a single ideal species in solution, and the molecular weight was allowed to vary during the fit. An M_r of 6422 (with 95% confidence limits of 5924 and 6911) was obtained, which is very close to the expected heterodimer value of 6303 calculated from mass spectrometry of the individual peptides. CD spectra for 100 μM fiber-producing mixtures (SAF-p1 with SAF-p2), and for blunt dimer-producing mixtures (SAF-p2 with SAF-p3), are shown in Figure 3c. For the blunt dimer-producing mixture, the shape and intensity of the CD spectrum were fully consistent with coiled-coil formation as designed. In contrast to the fiber-producing mixtures, the blunt dimer-producing mixtures showed no signs of maturation; that is, negligible spectral changes and no clouding of solutions occurred upon incubation. Interestingly, the intensity of the minimum near 222 nm, which is an accepted indicator of α-helical structure and degree of α-helical folding, was similar for both mixtures. This strongly supports the formation of α-helical structure as designed in the fiber-producing mixtures despite the spectral shifts observed upon maturation.

Linear Dichroism Spectroscopy. The CD data described above were consistent with the SAF design and suggested the formation of large α-helical assemblies. To test if elongated structures were being formed as designed, we utilized linear dichroism (LD) spectroscopy. Long polymers such as duplex DNA with ≥1000 base pairs can be oriented

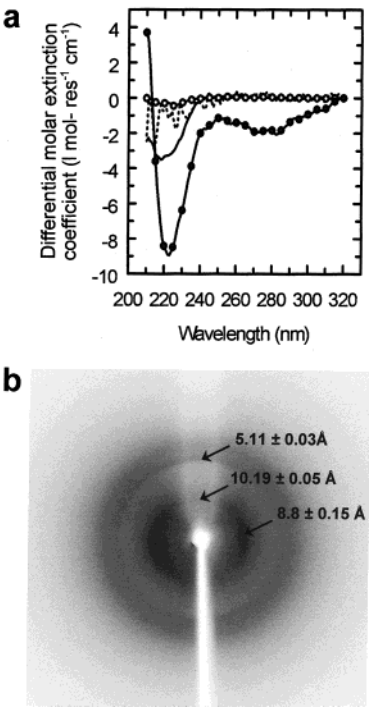

FIGURE 4: Spectroscopic and X-ray diffraction analysis of aligned fibers. (a) Linear dichroism (LD) spectra for 20 μM tropomyosin (—), a 10 μM mixture of SAF-p1 and SAF-p2 (---), and a matured 100 μM mixture of SAF-p1 and SAF-p2 in the absence (●) and presence (○) of 0.5 M KF. For clarity, only a fraction of the experimental data points are highlighted by the symbols (●) and (○). (b) X-ray fiber diffraction image collected from dried SAF-peptide fibers aligned vertically in the beam. The fibers were prepared as described under Experimental Procedures by mixing SAF-p1 with a version of SAF-p2 containing a mutation of Ala7 to Trp.

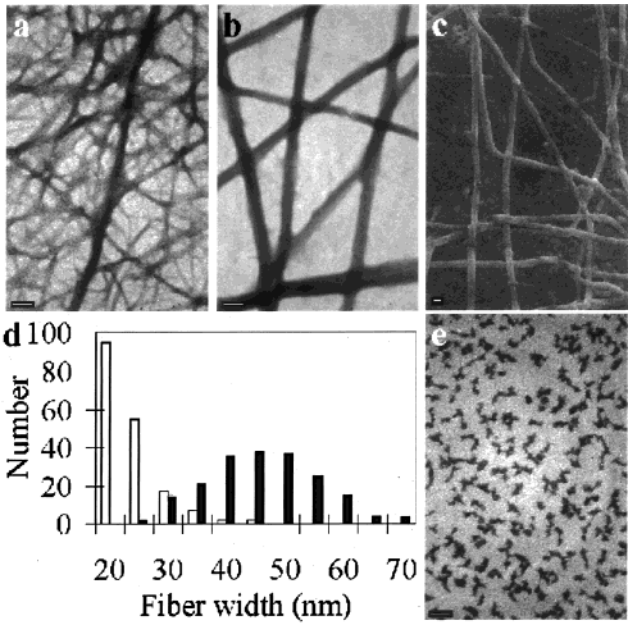

FIGURE 5: Assembly of synthetic protein fibers visualized directly by electron microscopy. TEM images of (a) a "fresh" fiber-producing mixture (SAF-p1 and SAF-p2) at 100 μM, (b) a "matured" fiber-producing mixture at 100 μM, and (e) a matured fiber-producing mixture at 100 μM incubated in the presence of 0.5 M KF. (c) SEM image of a matured fiber-producing mixture at 100 μM. In all panels, the white scale bars represent 100 nm. (d) Histograms showing the distribution of fiber widths determined using TEM for fresh (white bars) and matured (black bars) fiber-producing mixtures at 100 μM [a width value of "x" on the histogram includes all measurements from "(x − 5) to x" nm].

by shear flow. This effect can be monitored by LD spectroscopy provided that chromophores also become aligned by the flow (*29*, *37*); LD spectroscopy measures differences in absorption of light polarized parallel and perpendicular to the orientation axis. We found that tropomyosin, which is an extended dimeric coiled-coil approximately 42 nm in length, could be aligned to give a LD signal (Figure 4a). In contrast, LD signals were not detected in control experiments with fiber-producing mixtures at 10 μM (Figure 4a), or with the individual peptides at 100 μM (data not shown). However, a matured fiber-producing mixture at 100 μM gave a strong absorbance from the peptide backbone (210−240 nm) and some signal in the aromatic region (260−290 nm) during flow orientation (Figure 4a). These data demonstrated clearly that long structures were present and could be aligned in the matured 100 μM fiber-producing mixture.

X-ray Fiber Diffraction. The X-ray fiber diffraction pattern collected from SAF peptide fibers showed the following features (Figure 4b): (1) a sharp meridional (that is, parallel to the long fiber axis) reflection at 5.11 ± 0.03 Å; (2) the harmonic of this 5.11 reflection at 10.19 ± 0.05 Å; and (3) a stronger, more diffuse reflection centered at 8.8 ± 0.15 Å on the equator. These features are consistent with α-helical coiled-coils aligned with the fiber axis (*38*). The 5.1 Å meridional reflection corresponds to the pitch of the helices within the coiled-coils. The other expected reflection on the meridian—that is, that at 1.5 Å and corresponding to the rise per residue—lies out of the resolution of the current data sets, whereas the equatorial reflection reveals the mean distance between α-helical axes. This value at 8.8 Å is less than the observed value for keratin but falls within reported ranges for dimeric coiled-coil peptides (*39*, *40*).

Electron Microscopy. We used electron microscopy to visualize structures in the peptide preparations directly. No structures were visible up to 100 000 times magnification by transmission electron microscopy (TEM) either for the fiber-producing mixtures at 10 μM or for the individual peptides at 100 μM concentration (data not shown). Similarly, there was no evidence for fibrous structures in blunt dimer-producing mixtures at 100 μM, which were designed to form blunt-ended, nonextendible heterodimers. However, TEM of 100 μM fiber-producing mixtures revealed time-dependent formation of long fibrous structures, consistent with the CD and LD data. Fresh mixtures showed large numbers of extended fibers of various widths. The majority of these had diameters of about 20 nm (Figure 5a,d); finer fibers were present, but their widths could not be measured reliably. Images recorded for matured mixtures showed fewer fibers, but these were more distinct and thicker than those observed in the fresh mixture (Figure 5b,d). Scanning electron microscopy (SEM) of matured mixtures showed no evidence for fiber branching (Figure 5c). Rather, the fibers were simply intertwined as if layered on top of each other. It was not possible to follow the full length of fibers due to intertwining, but they were at least several hundred micrometers long. Although the density of fibers varied across the surface of the specimen grid, their diameters were surprisingly uniform in the matured samples (Figure 5d) with

a mean width of 43.3 nm (standard deviation 9.3 nm; 195 measurements). As the original design was for a longitudinally extended, two-stranded coiled-coil, the average diameter that we might have expected was about 2 nm. Therefore, the electron microscopy data suggested that the designed two-stranded coiled-coil fibers associated laterally into high-order assemblies.

DISCUSSION

To summarize, we have used the coiled-coil motif to demonstrate sticky-end-directed design and self-assembly of two short peptides to form a fiber. CD spectroscopy and X-ray fiber diffraction provided good evidence for coiled-coil formation as designed, and electron microscopy showed that the sticky-ends were responsible for fiber elongation as, by comparison, a mixture that yielded blunt-end dimers did not form fibers. Electron microscopy also revealed that the fibers were an order of magnitude thicker than originally anticipated.

The probable lateral association of the designed two-stranded fibers was curious because we did not knowingly design any features into the SAF peptides to foster it. This raised the following question: What interactions guided and stabilized the high-order assemblies? We propose that complementary features present in repeating structures of the type that we have designed will naturally promote fibrillogenesis. Any sequence feature present on the surface of the designed fiber—that is, a two-stranded coiled-coil as depicted in Figures 1b and 2a—by either, or both, of the constituent peptides will be repeated at regular intervals along its structure. The repeat length will be equal to the length of the peptides (i.e., about 4.2 nm for the 28-residue SAF peptides described), and the sequence motif will spiral around the fiber tracking the superhelix of the coiled-coil, which has a pitch of about 15 nm for a contiguous, heptad-based, dimeric structure (*41*). If another motif is present that is complementary to the first, fiber−fiber interactions may be promoted because the pitches of the complementary motifs on each fiber will match precisely. Once initiated, lateral association of fibers—i.e., fibrillogenesis—will be cemented by many regularly spaced interactions as in a crystal. As a result, the complementary interactions need only be weak because the stability of the fiber−fiber interaction rests on avidity rather than on making a small number of strong interactions. Provided that the components of the assembly can make more than one type of complementary surface, very extensive molecular assemblies may result.

In general terms, our comparison of sticky-end fiber-producing and blunt-end dimer-producing mixtures lends support to this fibrillogenesis model; periodic interactions are not possible with the latter. However, it is harder to disentangle the specific interactions that could have given rise to the large assemblies that we observed. Nonetheless, it is interesting to consider the likely candidates. We used electrostatic interactions to promote the elongation of fibers (Figure 1). These features would also create periodic and alternating patches of charge in the fibers provided that they are regular as envisaged (Figures 1b and 2a). Indeed, molecular modeling of the SAF sequences into an extended two-stranded coiled-coil highlighted potential complementary charge interactions on the surface of the fibers (Figure 2b). These charged patches may have guided and stabilized the high-order assemblies. Interestingly, similar features have been noted in several natural fibrous proteins and have been implicated in the assembly of protein and peptide filaments. Examples include intermediate filaments, which assemble into fibers at least 10 nm thick (*42, 43*), and small peptide designer systems that assemble into "macroscopic membranes" and "nanotapes" (*44, 45*). Consistent with this, we found that moderate concentrations of salt inhibited assembly of fibers and the proposed multi-fiber bundles in SAF peptide mixtures. First, CD spectra recorded for 100 μM fiber-producing mixtures with 0.5 M potassium fluoride had reduced helicity and showed no tendency to "mature" (Figure 3d). Second, the LD signal described previously for the matured 100 μM fiber-producing mixture was also lost when the experiments were repeated in the presence of salt (Figure 4). Finally, TEM images of 100 μM fiber-producing mixtures also showed that fibers were not formed in 0.5 M salt (Figure 5e).

Natural coiled-coils do form a variety of bundles, fibers, and high-order assemblies (*4, 16, 17*). We recognize that in some of these cases, and in other systems, globular head domains may mediate the assembly process (*17, 46, 47*). Nevertheless, our studies on a designer, model system suggest a possible mechanism for propagation of coiled-coil fibrillogenesis, which is consistent with available data on certain natural systems (*42, 43*). In addition, our arguments may extend to other natural and designer systems: in essence, any extended structure with identical, repeated, and regularly spaced subunits has the potential to associate to high-order assemblies if the subunits or low-order structures present complementary features as we have described. Moreover, because of the avidity effect, the complementary interactions need not be strong to promote such fibrillogenesis. It is intriguing that our designed fibers consistently assembled to (that is, appeared to stop assembling at) a diameter of about 43 nm. Furthermore, certain natural polymers with repeated subunits do not assemble laterally, e.g., actin. Therefore, rather than searching for stabilizing interactions that drive fibrillogenesis, a more pertinent question may be the following: What controls and limits the size of high-order assemblies formed by repeating structures of the type we describe?

ACKNOWLEDGMENT

We thank Jenny Lees for seeding the idea for this work; Chris Kowalczyk for peptide synthesis and mass spectrometry; Richard Sessions for help with the molecular modeling; Ben Luisi and Andrew Sharff for use of the X-ray facility in the Biochemistry Department, Cambridge; and Tim Clackson and Richard Sessions for their critical appraisals of the manuscript. Credits: D.N.W. and M.J.P. designed the SAF sequences; M.J.P. and D.N.W. conceived the experiments; G.M.S. and D.N.W. conducted preliminary CD studies; M.J.P. performed all of the experiments described herein; J.R.T. advised and helped with the EM studies; A.R. advised and helped with the LD work; M.S. performed the X-ray fiber diffraction studies; M.J.P. and D.N.W. co-wrote the manuscript.

REFERENCES

1. Kelly, J. W. (1998) *Curr. Opin. Struct. Biol. 8*, 101−106.

2. Gu, L.-Q., Braha, O., Conlan, S., Cheley, S., and Bayley, H. (1999) *Nature 398*, 686−690.
3. Drexler, K. E. (1999) *Trends Biotechnol. 17*, 5−7.
4. Lupas, A. (1996) *Trends Biochem. Sci. 21*, 375−382.
5. Harbury, P. B., Zhang, T., Kim, P. S., and Alber, T. (1993) *Science 262*, 1401−1407.
6. Woolfson, D. N., and Alber, T. (1995) *Protein Sci. 4*, 1596−1607.
7. Wagschal, K., Tripet, B., Lavigne, P., Mant, C., and Hodges, R. S. (1999) *Protein Sci. 8*, 2312−2329.
8. O'Shea, E. K., Rutkowski, R., and Kim, P. S. (1992) *Cell 68*, 699−708.
9. Vinson, C. R., Hai, T., and Boyd, S. M. (1993) *Genes Dev. 7*, 1047−1058.
10. Kohn, W. D., Kay, C. M., and Hodges, R. S. (1998) *J. Mol. Biol. 283*, 993−1012.
11. O'Shea, E. K., Rutkowski, R., and Kim, P. S. (1989) *Science 243*, 538−542.
12. O'Shea, E. K., Klemm, J. D., Kim, P. S., and Alber, T. (1991) *Science 254*, 539−544.
13. Kohn, W. D., and Hodges, R. S. (1998) *Trends Biotechnol. 16*, 379−389.
14. Schneider, J. P., Lombardi, A., and DeGrado, W. F. (1998) *Folding Des. 3*, R29−R40.
15. Harbury, P. B., Plecs, J. J., Tidor, B., Alber, T., and Kim, P. S. (1998) *Science 282*, 1462−1467.
16. Kreis, T., and Vale, R. (1999) *Guidebook to the Cytoskeletal and Motor Proteins*, Oxford University Press, Oxford.
17. Herrmann, H., and Aebi, U. (1998) *Curr. Opin. Struct. Biol. 8*, 177−185.
18. Knop, M., Pereira, G., and Schiebel, E. (1999) *Biol. Cell 91*, 291−304.
19. Marvin, D. A. (1998) *Curr. Opin. Struct. Biol. 8*, 150−158.
20. Steinmetz, M. O., Stoffler, D., Hoenger, A., Bremer, A., and Aebi, U. (1997) *J. Struct. Biol. 119*, 295−320.
21. Phillips, G. N., Fillers, J. P., and Cohen, C. (1986) *J. Mol. Biol. 192*, 111−131.
22. McLachlan, A. D., and Karn, J. (1983) *J. Mol. Biol. 164*, 605−626.
23. Palmer, S. J., Redfern, M. R., Smith, G. C., and Cox, J. P. L. (1998) *Nucleic Acids Res. 26*, 2560−2564.
24. Winfree, E., Liu, F., Wenzler, L. A., and Seeman, N. C. (1998) *Nature 394*, 539−544.
25. Ogihara, N. L., Weiss, M. S., DeGrado, W. F., and Eisenberg, D. (1997) *Protein Sci. 6*, 80−88.
26. Prive, G. G., Anderson, D. H., Wesson, L., Cascio, D., and Eisenberg, D. (1999) *Protein Sci. 8*, 1400−1409.
27. Kojima, S., Kuriki, Y., Yoshida, T., Yazaki, K., and Miura, K. (1997) *Proc. Jpn. Acad. Ser. B 73*, 7−11.
28. Offer, G., and Sessions, R. (1995) *J. Mol. Biol. 249*, 967−987.
29. Rodger, A., and Norden, B. (1997) *Circular Dichroism and Linear Dichroism*, Vol. 1, Oxford University Press, Oxford.
30. Johnson, M. L., Correia, J. J., Yphantis, D. A., and Halvorson, H. R. (1981) *Biophys. J. 36*, 575−588.
31. Serpell, L. C., Fraser, P. E., and Sunde, M. (1999) *Methods Enzymol. 309*, 526−536.
32. Gonzalez, L., Woolfson, D. N., and Alber, T. (1996) *Nat. Struct. Biol. 3*, 1011−1018.
33. Graddis, T. J., Myszka, D. G., and Chaiken, I. M. (1993) *Biochemistry 32*, 12664−12671.
34. Lumb, K. J., and Kim, P. S. (1995) *Biochemistry 34*, 8642−8648.
35. Long, M. M., Urry, D. W., and Stoeckenius, W. (1977) *Biochem. Biophys. Res. Commun. 75*, 725−731.
36. Masui, R., Mikawa, T., and Kuramitsu, S. (1997) *J. Biol. Chem. 272*, 27707−27715.
37. Bloemendal, M. (1994) *Chem. Soc. Rev. 23*, 265−273.
38. Rasmussen, R., Benvegnu, D., O'Shea, E. K., Kim, P. S., and Alber, T. (1991) *Proc. Natl. Acad. Sci. U.S.A. 88*, 561−564.
39. DeLano, W. L., and Brunger, A. T. (1994) *Proteins: Struct., Funct., Genet. 20*, 105−123.
40. Gonzalez, L. J., Brown, R. A., Richardson, D., and Alber, T. (1996) *Nat. Struct. Biol. 3*, 1002−1018.
41. Seo, J., and Cohen, C. (1993) *Proteins: Struct., Funct., Genet. 15*, 223−234.
42. Meng, J.-J., Khan, S., and Ip, W. (1994) *J. Biol. Chem. 269*, 18679−18685.
43. McLachlan, A. D., and Stewart, M. (1976) *J. Mol. Biol. 103*, 271−298.
44. Zhang, S., Holmes, T., Lockshin, C., and Rich, A. (1993) *Proc. Natl. Acad. Sci. U.S.A. 90*, 3334−3338.
45. Aggeli, A., Bell, M., Boden, N., Keen, J. N., Knowles, P. F., McLeish, T. C. B., Pitkeathly, M., and Radford, S. E. (1997) *Nature 386*, 259−262.
46. Tao, Y., Strelkov, S. V., Mesyanshinov, V., and Rossman, M. G. (1997) *Structure 7*, 789−798.
47. van Raaij, M. J., Mitraki, A., Lavigne, G., and Cusack, S. (1999) *Nature 401*, 935−938.

BI000246G